International Journal of Applied Engineering Research
ISSN 0973-4562 Volume 10, Number 12 (2015) pp. 30725-30744

http://www.ripublication.com

Comparative Numerical Analysis Of Heat Flux Measurement Over An Aerodynamics Vehicle Surface

Ashish Narayan and *Rakesh Kumar

*Research Scholar, *Assistant Professor*
Department of Mechanical Engineering, ISM Dhanbad
*E-mail: ashishnarayan2007@gmail.com, *rakeshkism@gmail.com*

Abstract

Measurement of transient surface temperature and heat flux is the major requirement in many scientific and engineering applications such as design of combustion chamber in internal combustion engines, design of systems/sub-systems like heat exchanger, steam/gas turbines and thermal protection systems for high speed Aerodynamic vehicles. It is measure in conduction, convection and radiation area. Convection is the concerted, collective movement of groups or aggregates of molecules within fluids (e.g., liquids, gases) and rheids, either through advection or through diffusion or as a combination of both of them. Convection of mass cannot take place in solids, since neither bulk current flows nor significant diffusion can take place in solids. Convective heat transfer may take the form of either forced or assisted convection, natural or free convection. Forced convection occurs when a fluid flow is induced by an external force, such as a pump, fan or a mixer. Natural convection is caused by buoyancy forces due to density differences caused by temperature variations in the fluid. At heating the density change in the boundary layer will cause the fluid to rise and be replaced by cooler fluid that also will heat and rise. This continues phenomena are called free or natural convection. Aerodynamic forces and fore-body convective surface heat transfer rates over a blunt cone measured at a nominal Mach number of 5 in the hypersonic flow. An aluminum model incorporating a three-component accelerometer-based balance system for measuring the aerodynamic forces. The normalized values of measured heat transfer rates at different angle of attack for different model. The aerodynamic and the heat transfer data presented here are very valuable for the validation of CFD codes used for the numerical computation of flow fields around hypersonic vehicles.

1. Introduction:

Flow is the mental State of operation in which a person performing an activity is fully immersed in a feeling of energized focus, full involvement, and enjoyment in the process of the activity. It has several sub-disciplines itself, including aerodynamics (the study of air and other gases in motion) and hydrodynamics (the study of liquids in motion). Flow is classified according to speed regime (Subsonic flows, transonic flows, Supersonic flows & hypersonic flow) aerodynamicists disagree on the precise definition of hypersonic flow. It is also depend on Mach number of the flow. Viscosity is associated with the frictional forces in a flow. In some flow fields, viscous effects are very small, and solutions may neglect to account for viscous effects. These approximations are called in viscid flows. Flows for which viscosity is not neglected are called viscous flows. If Mach number is below unity then the flow is called as subsonic. Sonic flow has Mach number exactly equal to one however flow in the narrow range of Mach number between 08-1.2 is called as transonic flow. When the flow Mach number exceeds beyond 1 then flow is called as supersonic flow. When flow speed exceeds five times the sound speed, it is treated as hypersonic flow.

"Aerodynamic heating" is one of the key considerations for the design of high speed vehicles and the prediction of surface heat fluxes on the aerodynamic surfaces becomes crucial parameter. In the design aspects of high speed flow, a 'stagnation point' occurs at some point on the surface of the body, where the fluid is brought to rest. In other words, the fluid velocity becomes zero and all the kinetic energy is converted into heat energy. Obviously, the heat flux is the maximum at of the body, where the fluid is brought to rest. In other words, the fluid velocity becomes zero and all the kinetic energy is converted into heat energy. Obviously, the heat flux is the maximum at this point leading to a very high value of temperature and pressure. As a quantitative estimate, [1] proposed the energy balance using the first law of thermodynamics, when a slug of mass (m), moving at velocity (V) is brought to rest. It leads to the fact that the entire kinetic energy is converted to heat energy (Q) as given below;

$$\frac{1}{2}mV^2=Q \Rightarrow \frac{1}{2}V^2=\frac{Q}{m} \tag{1}$$

For a sonic velocity of 340 m/s, the specific thermal load (Q /m) is expected to be 58kJ/kg and it is interpreted as the stagnation heating rate. If the specific is denoted as C_p, then the above equation can be used to obtain the stagnation temperature.

$$T_0=\frac{V^2}{2C_p} \tag{2}$$

Stagnation point is the location on a body that experiences maximum temperature and heat flux as compared to other locations. Normally, the temperature at the stagnation point is measured through surface thermometry methods like thin film gauges and coaxial surface junction thermocouple sensors. Some of the

resistance temperature detector sensors are thin film resistance thermometer [2 - 3], coaxial thermocouple [4] and temperature sensitive paint [5 - 6]. Different techniques to heat models prior to arrival of the test flow in blow down wind tunnels have also been discussed been blow down tunnels [7 - 8]. All of these devices or methods have significant deficiencies which could possibly contribute to degradation of the accuracy of the measurement. [9] used a fast response calorimeter type heat transfer gauge with sputtered thin film platinum thermometer to carry out the measurements in a hotshot tunnel.[10] Developed and investigate the application of high speed imaging and luminescent coating techniques to measure full field surface heat transfer rates for indented cone model. A new type of surface junction thermocouple sensor has been developed by which has a response time in the order of microseconds and is suitable for measuring large transient surface heat fluxes in wind tunnels [11]. Traditional optical methods such as liquid crystals have been attempted to measure heat transfer rates because of short test time available in impulse facilities [12]. There are other techniques used to view the thermal imaging of the full field are, thermal paints [13], infrared thermography [14] and thermo-graphic phosphors [15]. The thin film sensors made by vacuum deposition of thin layer of platinum on a macor substrate is used to measure the stagnation point heat flux in a shock tunnel [16]. They compared the results with analytic expressions for stagnation point heat flux value [17] and with numerical methods.

2. Measurements of Stagnation Point Heat Fluxes:

Air is composed of molecules that are moving about in a random motion with different instantaneous velocities and energies at different time intervals. However over a period of time, the average molecular velocity and energy can be defined and for a perfect gas, they are functions of the temperature only. Flow exits the reservoir through the nozzle if the back pressure is less than the reservoir pressure. Further, the maximum velocity of the fluid exists at the nozzle throat where the area is smallest. When the back pressure is further decreased, fluid exits the reservoir more rapidly. Eventually, the velocity at the throat reaches the sonic velocity, for which flow Mach number is unity (M =1). Further, decrease in back pressure will not increase the flow rate and the nozzle is said to be choked. This principle is used here to obtain the sonic jet by maintain the appropriate pressure ratio [18]. An isentropic relation for compressible flow exists to obtain the ratios of stagnation to static flow conditions for temperature and pressure.

$$\frac{T_0}{T_\infty} = 1 + \frac{\gamma - 1}{2} M^2 \tag{3}$$

$$\frac{P_0}{P_\infty} = \left(1 + \frac{\gamma - 1}{2} M^2\right)^{\frac{\gamma}{\gamma - 1}} \tag{4}$$

$$M=\frac{V_\infty}{a}=\frac{V_\infty}{\sqrt{\gamma RT}} \tag{5}$$

Where, T_0 and P_0 are total pressure and temperature. T_∞ , P_∞ and V_∞ are stream temperature, pressure and velocity, γ is the specific heat ratio, a is the speed of sound in the medium, R is gas constant, M is Mach number. For air (γ =1.4) , if the sonic flow has to occur, the above equations can be simplified to obtain the stagnation to static pressure and temperature ratios as given below;

$$\frac{T_0}{T_\infty}=1.2;\ \frac{P_0}{P_\infty}=1.9 \tag{6}$$

In any type of flow like Sonic and Hypersonic depend on the Mach number, Mach number varies by the composition of the surrounding medium and also by local conditions, especially temperature and pressure. The Mach number can be used to determine if a flow can be treated as an incompressible flow.Note that the dynamic pressure can be found as:

$$q=\frac{\gamma}{2}pM^2 \tag{7}$$

Assuming air to be an ideal gas, the formula to compute Mach number in a subsonic compressible flow is derived from Bernoulli's equation for M < 1.

$$M=\sqrt{\frac{2}{\gamma-1}\left[\left(\frac{q_c}{p}+1\right)^{\frac{\gamma-1}{\gamma}}-1\right]} \tag{8}$$

q_c is impact pressure (dynamic pressure),

p is static pressure and

γ is the ratio of specific heat of a gas at a constant pressure to heat at a constant volume (1.4 for air).

The formula to compute Mach number in a supersonic compressible flow is derived from the Rayleigh Supersonic Pitot equation:

$$\frac{q_c}{p}=\left[\frac{\gamma+1}{2}M^2\right]^{\left(\frac{\gamma}{\gamma-1}\right)}\cdot\left[\frac{\gamma+1}{\left(1-\lambda+2\gamma M^2\right)}\right]^{\frac{1}{\lambda-1}} \tag{9}$$

a point in the field a flow about a body where the fluid particles have zero velocity with respect to the body.

In fluid mechanics a stagnation point is a point in a flow field where the local velocity of the fluid is zero. Stagnation points exist at the surface of objects in the flow field, where the fluid is brought to rest by the object. The Bernoulli's equation shows that the static pressure is highest when the velocity is zero and hence static pressure is at its maximum value at stagnation points. This static pressure is called the stagnation pressure.

Therefore,

P(static) + Kinetic Energy = constant

P(static) + 0 = constant

Therefore

P(static) = Maximum = stagnation pressure

The measurement of heat transfer rates to the aerodynamic surfaces and high-speed flow environments are very important in the design of hypervelocity aerodynamic vehicles [19 - 20]. Hypersonic and re-entry vehicles are exposed to high temperatures and large temperature gradients as they travel through the atmosphere. Previous launch vehicles relied on thermal protection systems to handle thermal loads while the structure supported aerodynamic loads. Future launch vehicle designs will likely use non-insulated hot structures and multifunctional structures that sustain both thermal and aerodynamic loads simultaneously. Finite element methods are needed to predict accurately the thermal and structural response of these types of structures [21]. The finite element integrals containing the thermal conductivity are integrated using Gaussian quadrature. The surface heat fluxes are predicted from the transient temperatures by appropriate one-dimensional heat conduction modeling for semi-infinite body. The important parameter for the development of successful hypersonic vehicles is thermal protection system and for validating the numerical codes. The flow field of a vehicle that flies at hypersonic speeds is one in which high temperature gas effects strongly influence the forces and loads acting on the surface. Pressure distribution on the surface is required for estimating the structural loads and deciding on the provisions for venting [22-23]. In Aerodynamics shape assessing the accuracy of computational fluid dynamics (CFD) for applications in sports aerodynamics, for example for drag predictions of swimmers, cyclists or skiers, by evaluating the applied numerical modeling techniques by means of detailed validation experiments.

3 Numerical Modeling of Cone Spherical Shape Model for Four Different Models: The ever increasing advances in computer technology have enabled many in science and engineering fields to apply numerical methods for simulating physical phenomena. Numerical analysis is the study of algorithms that use numerical approximation for the problems of mathematical analysis (as distinguished from discrete mathematics). These methods are often divided into elementary ones such as finding the root of an equation, integrating a function or solving a linear system of equations to intensive ones like the finite element method. The overall goal of the

field of numerical analysis is the design and analysis of techniques to give approximate but accurate solutions for complicated problems. In this work we are taking the one model which is develop with the help of Catia V5R18 Software which is having shape like cone spherical (similar to the front part of aerodynamics) which is having dimension given in Fig.2, 10, 18 & 26. Fig.3, 12, 19 & 27 shows the 3-D model of the cone spherical shape model.

After creating the 3D modal we are doing the meshing (Discretisation of the modal or geometry) with the help of ANSYS workbench software for all the Cases.

The mesh size has been kept finer near the body walls, so as to capture the gradients accurately with the minimum side of a cell. The computational analysis has also been carried out for the hot air flow based experiments using commercial package ANSYS Fluent -14 in the two stages for all four cases. In the first stage, a computational domain and meshing of cone spherical shape has been prepared in a flow field by using ANSYS Workbench as shown in Fig-4, 13, 21 & 29, through which a highly compressed air exhausts to the atmosphere. Referring to the Fig. 5, 12, 20 & 28. After meshing the component we are doing the analysis with the help of ANSYS Fluent -14 to give the analysis report. The boundary conditions used in the simulation are given in Table 1for all four cases are the same.

Table1: Boundary Condition of the Flow Field

Mach Number	5
Inlet Pressure or Stagnation Pressure	30 bars
Inlet Temperature	310k
Outlet Temperature or Stagnation Temperature	At ATP

A pressure far field includes the free stream and inlet to the computational domain. Wall is kept as adiabatic with no slip condition. Pressure outlet includes the exit from the computational domain. The results are obtained for pressure and velocities flow fields as shown in Figs. 6, 14, 22 & 30 and 7, 15, 23 & 31. It is seen that indicate that pressure of the fluid is constant through the cone spherical shape model but at a certain distance from the nozzle tip, maximum value of jet is observed. At this point, the kinetic energy is the maximum and is considered as the optimum location of stagnation probe from Fig. 6, 14, 22 & 30. The velocity contour indicates that pressure of the fluid particle is constant through the cone spherical shape model and gradually reduces at the point nozzle tip velocity is zero (stagnation point development) from Fig. 7.

It is seen that indicate that density of the fluid is constant through the cone spherical shape model but at a certain distance from the nozzle tip, maximum value of jet is observed from Fig. 8, 16, 24 & 32. It is seen that indicate that temperature of the fluid is constant through the cone spherical shape model but at the end part of the model maximum value of temperature is observed from Fig. 9, 17, 25 & 33.

4 Comparative Numerical Analysis of cone spherical shape model for different Cases

4.1 Pressure Distribution for Lower and Upper Wall:

In the present study, a cold and heated airfoil is used in order to test the effect of flow characteristics over the airfoil at different angles of attack for both Lower and Upper wall of the cone spherical shape of the body in Fig. 34 &35. We found that in Upper wall Case 3 is having maximum pressure and for Lower wall Case 2 is having the maximum pressure. As the angles of attack increases, the main flow separates from the upper surface because the shape downstream of the foil shoulder is such as to produce a severe rate of pressure rise leads to boundary layer separation and consequently to a larger pressure distribution. For lower wall as the angles of attack increases, lower the pressure distribution.

4.2 Total Temperature Distribution for Lower and Upper Wall:

In the present study, a cold and heated airfoil is used in order to test the effect of flow characteristics over the airfoil at different angles of attack for both Lower and Upper wall of the cone spherical shape of the body in Fig. 36 & 37. We found that in Upper wall Case 3 is having maximum Total Temperature and for Lower wall Case 2 is having the maximum Total Temperature. As the angles of attack increases, the main flow separates from the upper surface because the shape downstream of the foil shoulder is such as to produce a severe rate of temperature rise leads to boundary layer separation and consequently to a larger temperature distribution. For lower wall as the angles of attack increases, lower the temperature distribution.

4.3 Density for Lower and Upper Wall:

In the present study, a cold and heated airfoil is used in order to test the effect of flow characteristics over the airfoil at different angles of attack for both Lower and Upper wall of the cone spherical shape of the body in Fig. 38 & 39. We found that in Upper wall Case 2 is having maximum Density and for Lower wall Case 2 is also having the maximum Density. As the angles of attack increases, the main flow separates from the upper surface because the shape downstream of the foil shoulder is such as to produce a severe rate of density rise leads to boundary layer separation and consequently to a lower density distribution. For lower wall as the angles of attack increases, lower the density distribution.

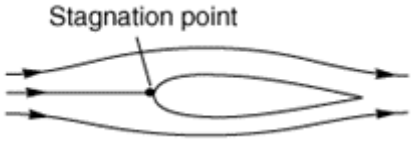

Fig.1: Stagnation Point Representation

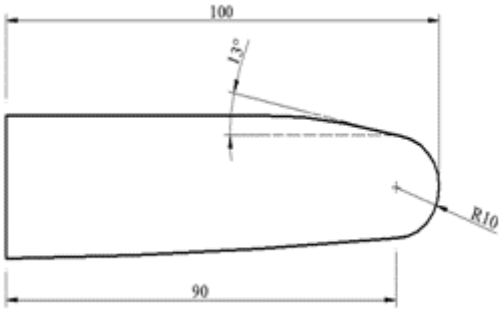

Fig.2: 2D Dimension of the (Case1) Cone Spherical Shape Model

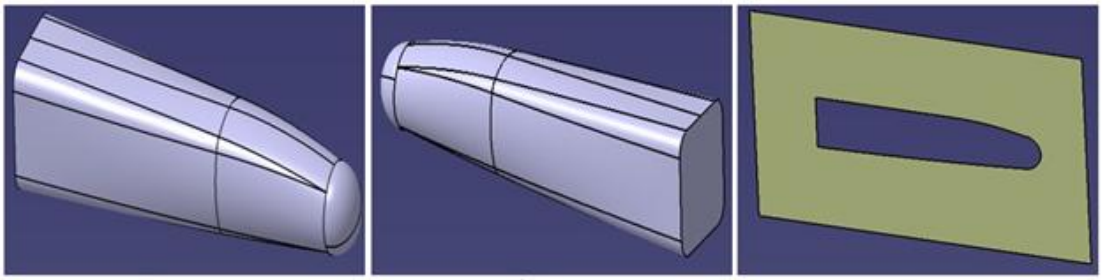

Fig. 3 (a - c): 3D Modal of (Case 1) the Cone Spherical Shape Model

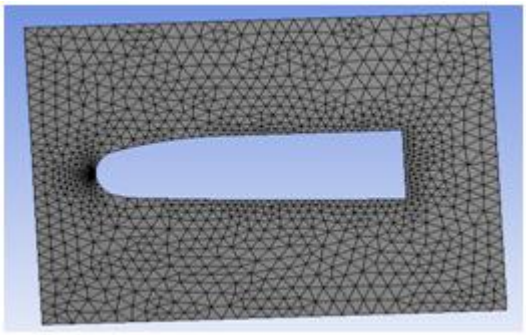

Fig. 4: Mesh of the (Case1) Cone Spherical Shape Model

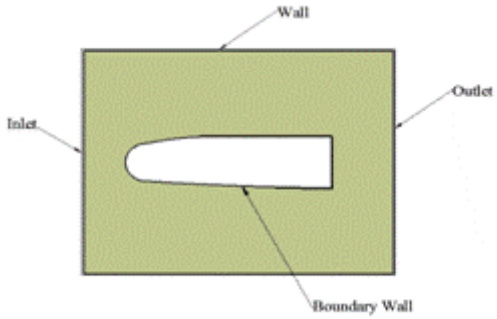

Fig. 5: Computational Model of a Flow Field (Case1)

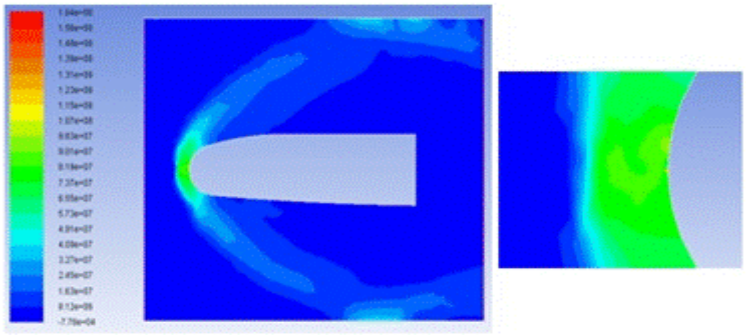

Fig. 6: Contour of Pressure distribution along the direction of flow field

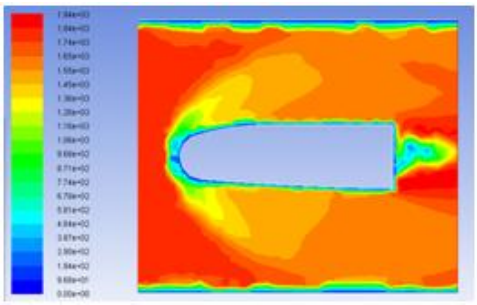

Fig. 7: Contour of Velocity distribution along the direction of flow field

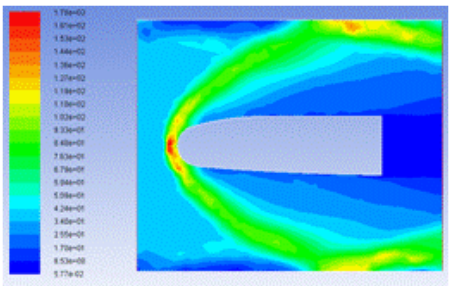

Fig. 8: Contour of Density distribution along the direction of flow field

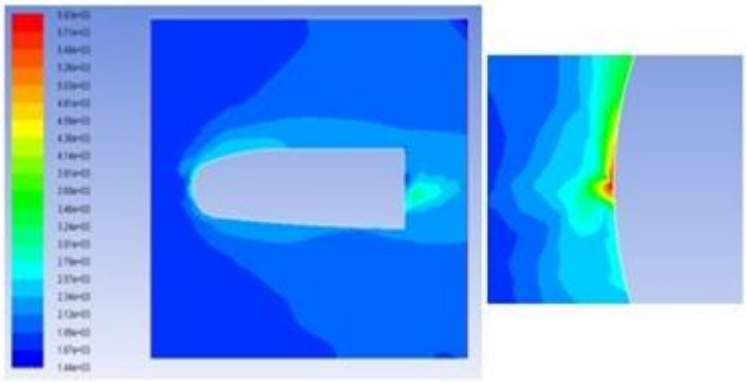

Fig. 9: Contour of Temperature distribution along the direction of flow field

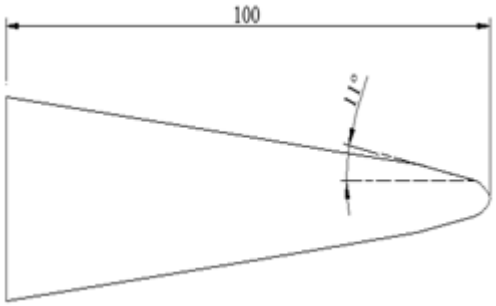

Fig.10: 2D Dimension of the (Case2) Cone Spherical Shape Model

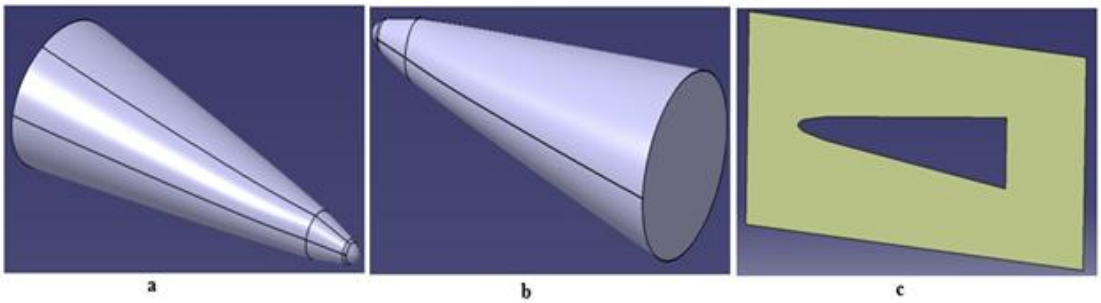

Fig. 11 (a - c): 3D Modal of (Case 2) the Cone Spherical Shape Model

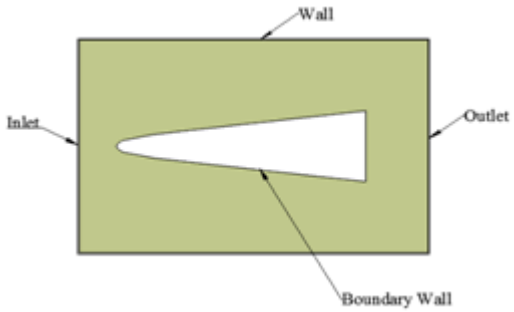

Fig. 12: Computational Model of a Flow Field (Case2)

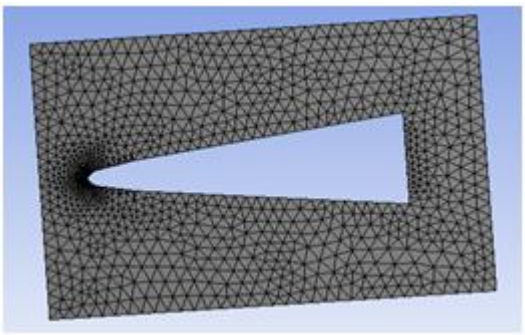

Fig. 13: Mesh of the (Case2) Cone Spherical Shape Model

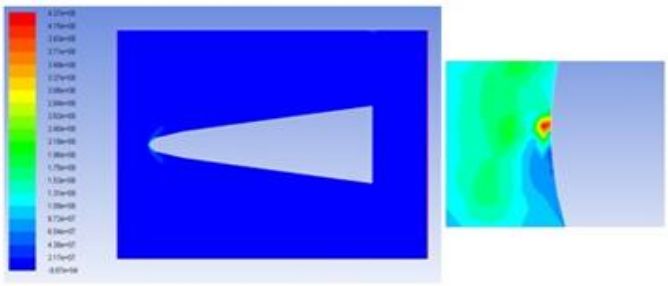

Fig. 14: Contour of Pressure distribution along the direction of flow field

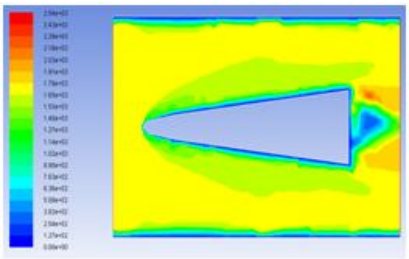

Fig. 15: Contour of Velocity distribution along the direction of flow field

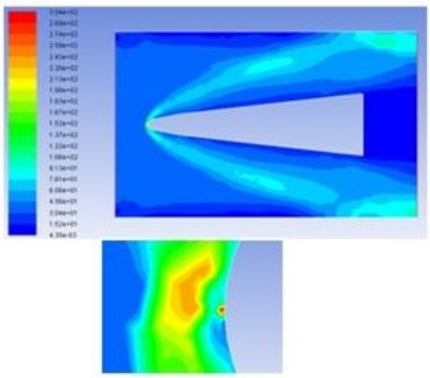

Fig. 16: Contour of Density distribution along the direction of flow field

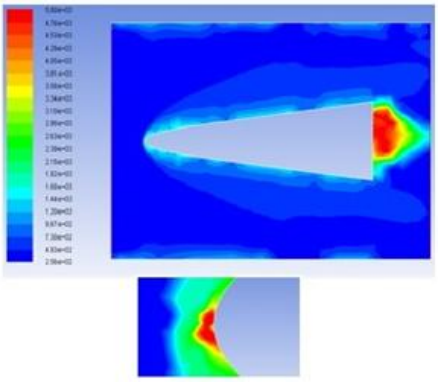

Fig. 17: Contour of Temperature distribution along the direction of flow field

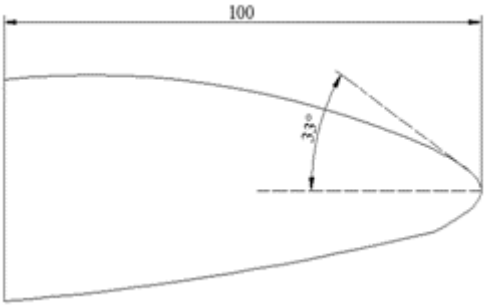

Fig.18: 2D Dimension of the (Case3) Cone Spherical Shape Model

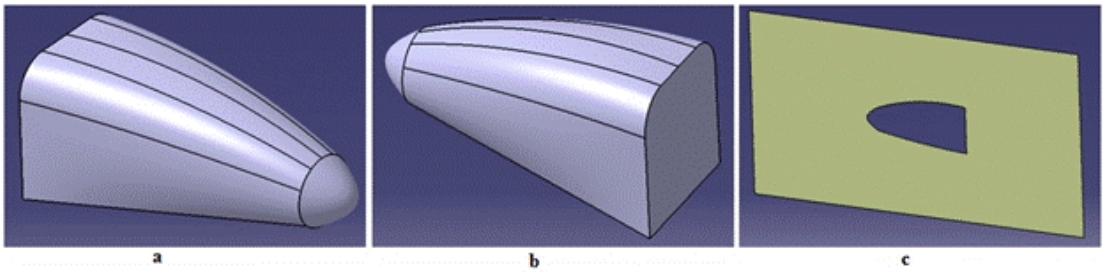

Fig. 19 (a - c): 3D Modal of (Case 3) the Cone Spherical Shape Model

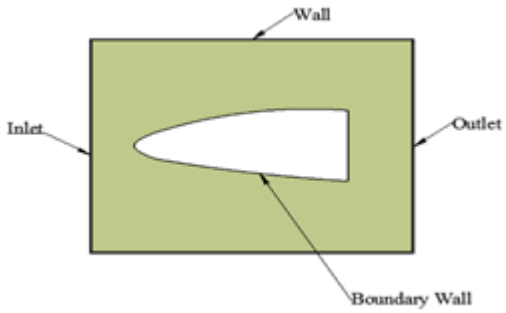

Fig. 20: Computational Model of a Flow Field (Case3)

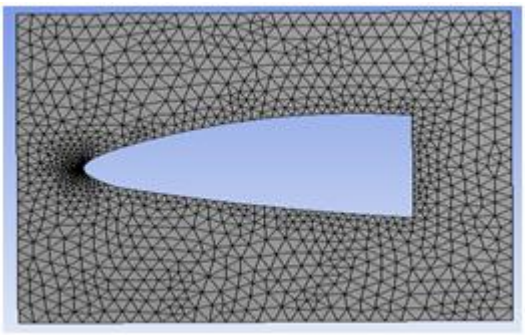

Fig. 21: Mesh of the (Case3) Cone Spherical Shape Model

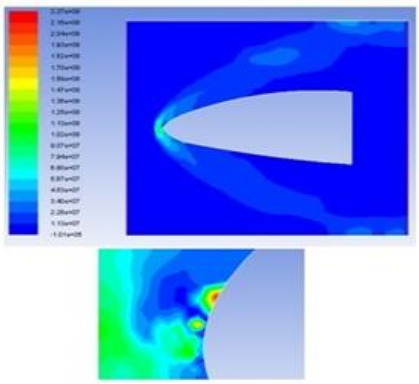

Fig. 22: Contour of Pressure distribution along the direction of flow field

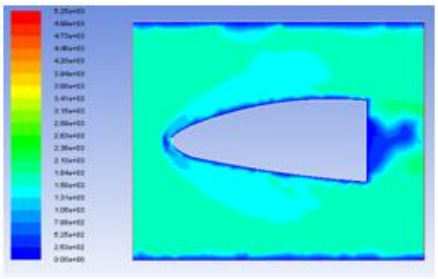

Fig. 23: Contour of Velocity distribution along the direction of flow field

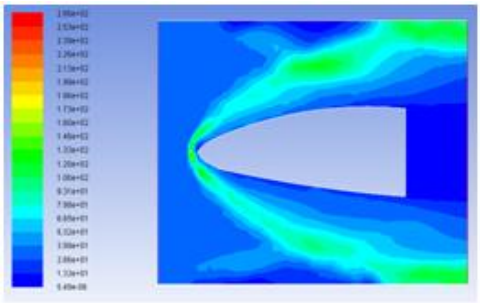

Fig. 24: Contour of Density distribution along the direction of flow field

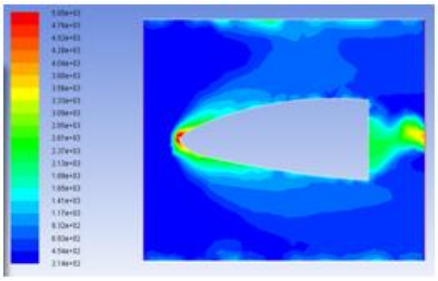

Fig. 25: Contour of Temperature distribution along the direction of flow field

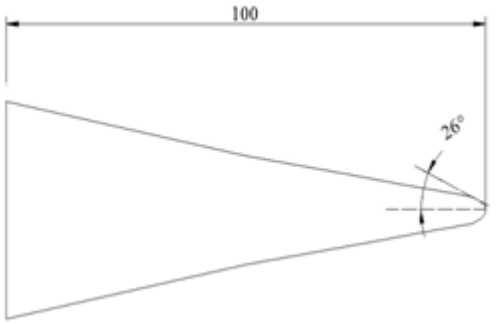

Fig.26: 2D Dimension of the (Case4) Cone Spherical Shape Model

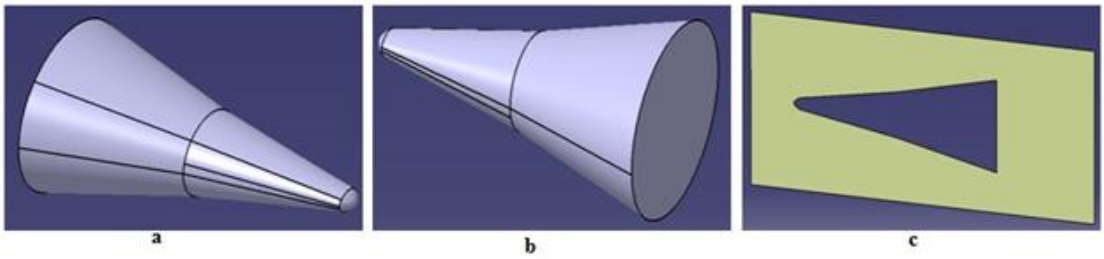

Fig. 27 (a - c): 3D Modal of (Case 4) the Cone Spherical Shape Model

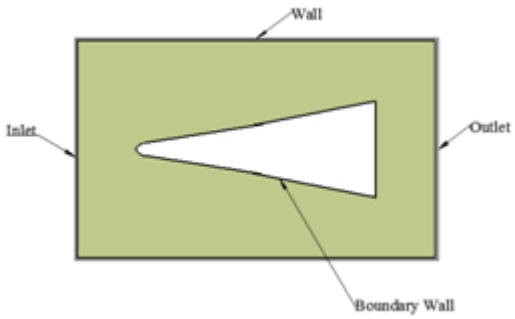

Fig. 28: Computational Model of a Flow Field (Case4)

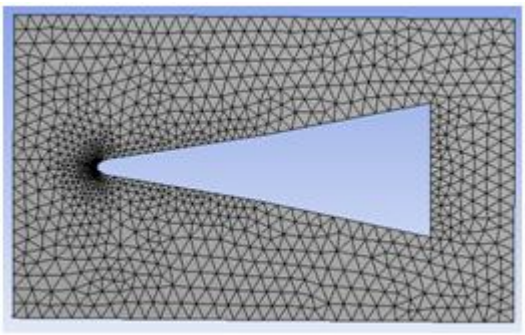

Fig. 29: Mesh of the (Case 4) Cone Spherical Shape Model

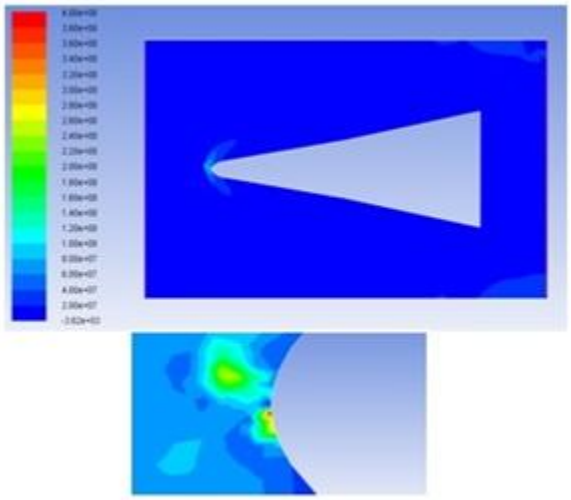

Fig. 30: Contour of Pressure distribution along the direction of flow field

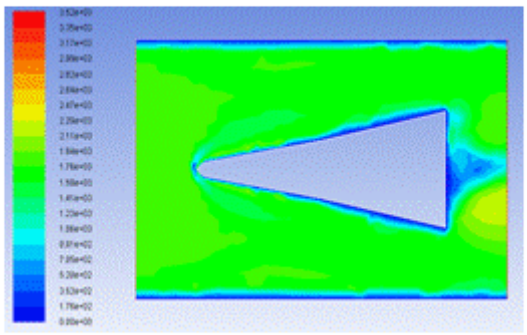

Fig. 31: Contour of Velocity distribution along the direction of flow field

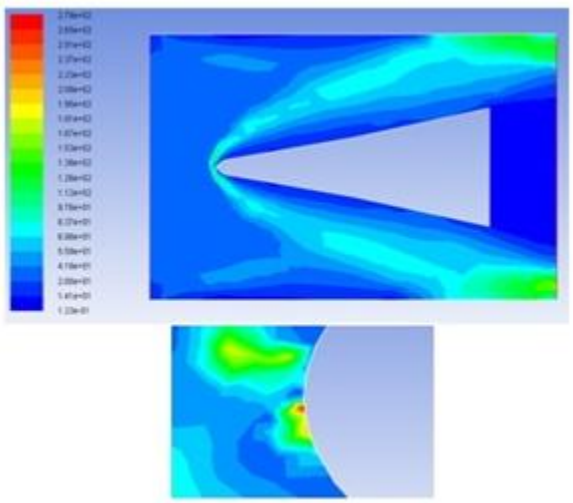

Fig. 32: Contour of Density distribution along the direction of flow field

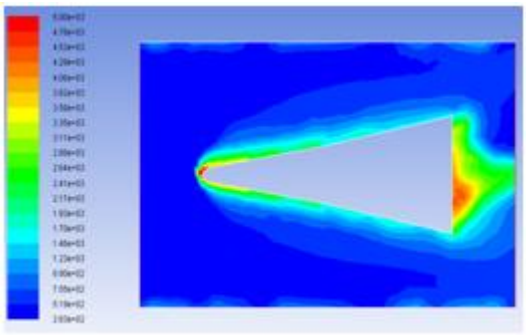

Fig. 33: Contour of Temperature distribution along the direction of flow field

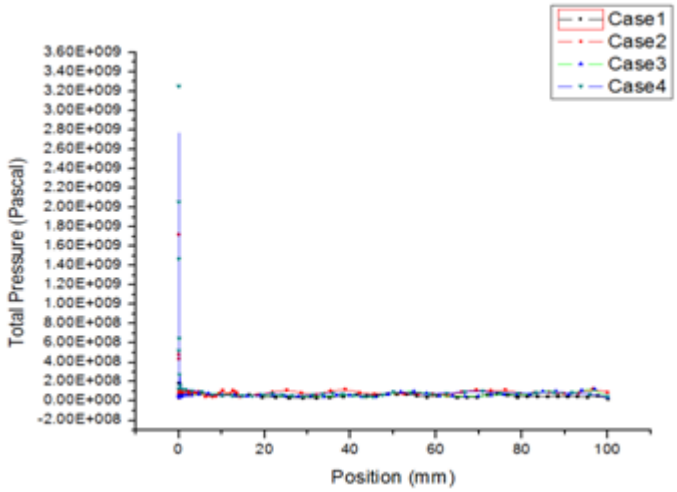

Fig. 34: Total Pressure Distribution for Lower Wall for all cases

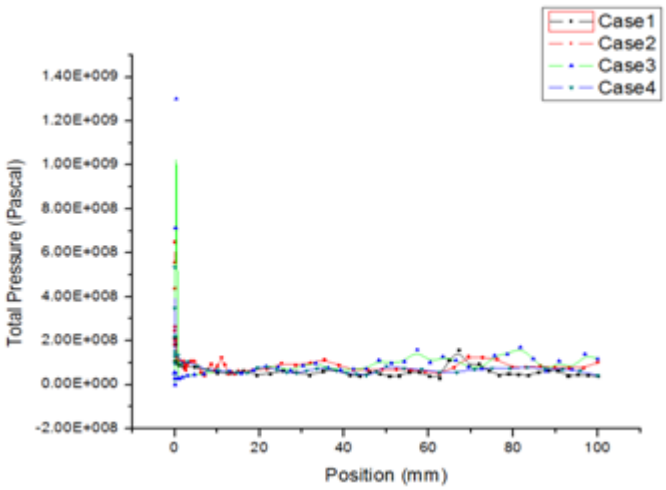

Fig. 35: Total Pressure Distribution for Upper Wall for all cases

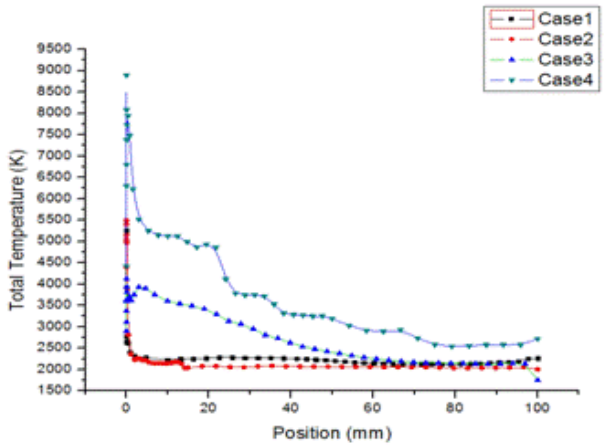

Fig. 36: Total Temperature Distribution for Lower Wall for all cases

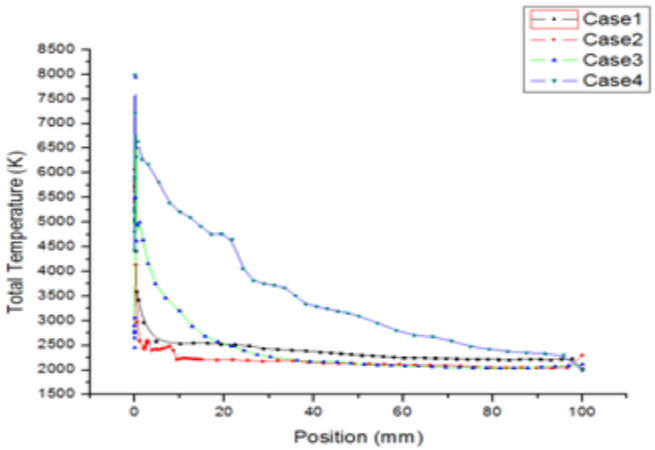

Fig. 37: Total Temperature Distribution for Upper Wall for all cases

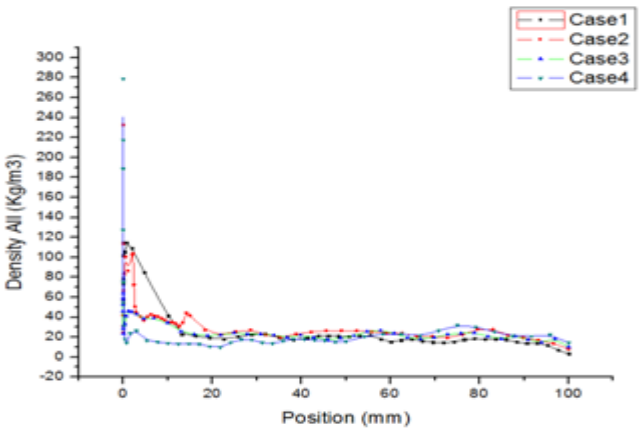

Fig. 38: Density All Distribution for Lower Wall for all cases

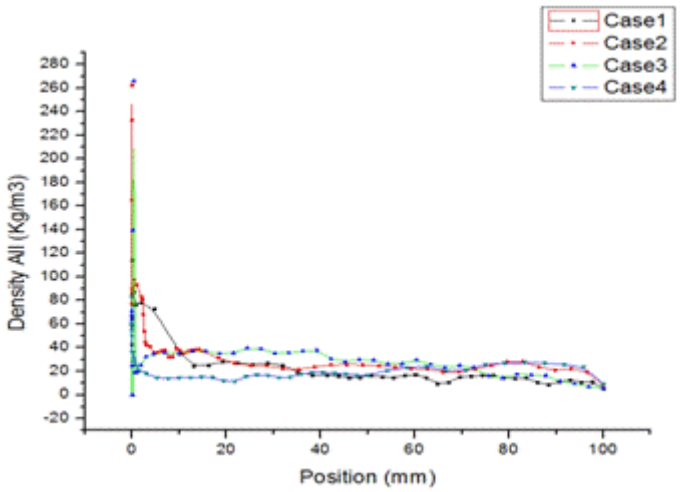

Fig. 39: Total Temperature Distribution for Upper Wall for all cases

5 Conclusions

In this analysis we conclude that the numerical simulation of the cone spherical shape model is safe for the Mach number of 5 which a highly compressed air exhausts to atmosphere. In order to evaluate the performance of the heat transfer gauges, the simulations are performed to measure stagnation point heat flux rate. All the analysis results are validated through numerical simulation with reasonable accuracy. These heat transfer gauges find applications to capture transient temperature in the combustion chambers of internal combustion engines and gas turbine blades etc. When mounted in flush on aerodynamic surfaces, they are used to record surface temperatures high speed air flows in short duration impulse facilities such as shock tunnels, wind tunnels etc. The flow and heat transfer characteristics of aerofoil were the angle of attack is varied in the range of $0^o \leq \alpha \leq 33^o$. From the flow characteristics, it is concluded higher the angle of attack higher pressure distribution, higher temperature distribution and lower density distribution for Upper layer of the wall in the same manner we conclude that for lower wall if we increases angle of attack lower pressure distribution, lower temperature distribution and lower density distribution.

References:

1. Hankley WL (1989) Re-entry aerodynamics, AIAA Education Series, 1- 22.
2. Miller CG (1981) Comparison of thin film resistance heat transfer gauges with thin skin transient calorimeter gages in conventional hypersonic wind tunnels, NASA Technical Memorandum, 83197, December 1981.
3. Wannenwetsch GD (1985) Measurements of wing leading edge heating rates on wind tunnel models using the thin film technique, AIAA Journal, 8: 983-972.

4. Kidd CT (1990) Recent developments in high heat flux measurement technique at the AEDC, Proceedings of the 36th International Instrumentation Symposium, Instrument Society of America, USA, 6-10 May, 1990, pp. 477-492.
5. Mosharov V, Orlov A and Radchenko V (2003) Temperature sensitive paint for heat transfer measurement in short duration wind tunnels, 20th International Congress on Instrumentation in Aerospace Simulation Facilities (ICIASF), 25-29 August 2003, 8: 351-356.
6. Nagai H, Oumi S, Asai K and Nakaita K (2006) Effect of temperature sensitive paint layer on global heat transfer measurement in hypersonic flow, Int. J. Visualization Society of Japan, 26: 201-204.
7. Lee Y, Settles GS and Horstman CC (1994) Heat transfer measurements and computations of swept shock wave/boundary layer interactions, AIAA Journal, 32 (4): 726-734.
8. Martinez BR, Lock GD and Jones TV (1995) Heat transfer measurements in an annular cascade of transonic gas turbine blades using the transient liquid crystal technique, Int. J. Turbo Machinery, 117: 425-431.
9. Widhopf GF (1971) Turbulent heat transfer measurements on a blunt cone at angle of attack, AIAA Journal, 9(8): 1574-1580.
10. Hubner JP, Carroll BF and Schanze KS (2002) Heat transfer measurements in hypersonic flow using luminescent coating techniques, Int. J. Thermo Physics and Heat Transfer, 16(4): 516-522.
11. Sanderson SR and Sturtevant B (2002) Transient heat flux measurement using a surface junction thermocouple, AIP Review of Scientific Instruments, 73 (7): 2781-2787.
12. Merski NR (1998) Reduction and analysis of phosphor thermography data with the one dimensional heat software package, AIAA Paper, pp. 98-712.
13. Asai K, Kunimasu T and Iijima Y (1997) Visualization of the quiet test region in a supersonic wind tunnel using luminescent paint, 17th International Congress on Instrumentation in Aerospace Simulation Facilities, The University of Michigan, USA, September 29 – October 2, 1997.
14. Luca LD, Guglieri G, Cardone G and Carlomagno GM (1995) Experimental analysis of surface flow on a delta wing by infrared thermography, AIAA Journal, 33: 1510-1512.
15. Micol JR (1995) Aero-thermodynamic measurement and prediction for a modified orbiter at Mach 6 and 10 in air, Int. J. Spacecraft and Rockets, 32 (5): 737-748.
16. Reddy KPJ, Saravanan S, Jagadeesh G (2009) Convective heat transfer rate distributions over a missile shaped body flying at hypersonic speeds, Int. J. Experimental Thermal and Fluid Science, 33: 782-790.
17. Fay JA and Riddell FA (1958) Theory of stagnation point heat transfer in dissociated air, Int. J. Aeronautical Sciences, 25: 73-85.
18. Anderson JD (1990) Modern compressible flow, Tata McGraw-Hill Edition.

19. R. Kumar and N. Sahoo (2012) Design, Fabrication and Sensitivity Analysis of the Resistance Temperature Detector Thin Film Sensors, International Journal of Mechanical and Industrial Engineering, 2(4): 20-25.
20. J. C. Sanders, (2002), Nonlinear, Transient Conduction Heat Transfer Using a Discontinuous Galerkin Hierarchical Finite Element Method, the College of New Jersey.
21. N. Sahoo, S Saravanan, G Jagadeesh and K P J Reddy (2006), Simultaneous measurement of aerodynamic and heat transfer data for large angle blunt cones in hypersonic shock tunnel, Sadhana 31(5): 557–581.
22. R. Kumar, N. Sahoo and V. Kulkarni (2012) Conduction based calibration of handmade platinum thin film heat transfer gauges for transient measurements, International Journal of Heat and Mass Transfer, 55: 2707–2713.
23. M. Divakaran and J. Kurian, (2008) Experimental Investigation of Heat Flux and Pressure on Sphere-Cone-Flare Model at Hypersonic speeds, International Conference on Aerospace Science and Technology.